LETTERS

Thermal vestige of the zero-temperature jamming transition

Zexin Zhang[1]*, Ning Xu[1,2]*, Daniel T. N. Chen[1], Peter Yunker[1], Ahmed M. Alsayed[1], Kevin B. Aptowicz[3], Piotr Habdas[4], Andrea J. Liu[1], Sidney R. Nagel[2] & Arjun G. Yodh[1]

When the packing fraction is increased sufficiently, loose particulates jam to form a rigid solid in which the constituents are no longer free to move. In typical granular materials and foams, the thermal energy is too small to produce structural rearrangements. In this zero-temperature ($T = 0$) limit, multiple diverging[1–8] and vanishing[2,9,10] length scales characterize the approach to a sharp jamming transition. However, because thermal motion becomes relevant when the particles are small enough, it is imperative to understand how these length scales evolve as the temperature is increased. Here we used both colloidal experiments and computer simulations to progress beyond the zero-temperature limit to track one of the key parameters—the overlap distance between neighbouring particles—which vanishes at the $T = 0$ jamming transition. We find that this structural feature retains a vestige of its $T = 0$ behaviour and evolves in an unusual manner, which has masked its appearance until now. It is evident as a function of packing fraction at fixed temperature, but not as a function of temperature at fixed packing fraction or pressure. Our results conclusively demonstrate that length scales associated with the $T = 0$ jamming transition persist in thermal systems, not only in simulations but also in laboratory experiments.

The onset of the arrested dynamics associated with jamming depends on an interplay between packing constraints, thermal energy and applied forcing[11,12]. This behaviour is illustrated in the schematic jamming phase diagram of Fig. 1, where the zero-temperature jamming transition point for finite-range, repulsive spheres[2] is labelled 'J'. It has been unclear how this zero-temperature transition affects behaviour at non-zero temperature. To explore its influence, we used experiments and numerical simulations to study structure and dynamics at non-zero temperature in the vicinity of Point J.

At zero temperature, the average number of touching neighbours per particle, Z, jumps discontinuously at Point J, from $Z = 0$ to the minimum number required for mechanical stability, Z_c, when the packing fraction, ϕ, is increased through the transition at ϕ_c (refs 1, 2 and 13). This discontinuity produces a δ-function in the first peak of the pair-correlation function $g(r)$, which measures the probability of finding another particle at distance r given one at the origin[2,10]. Numerical simulations at $T = 0$ confirm that g_1, the height of the first peak in $g(r)$, diverges as $g_1 \approx |\phi - \phi_c|^{-1.0}$ as ϕ_c is approached both from above[2,10] and below[9]. The overlap distance L_{ov} (that is, the left-hand width of the first peak) is directly related to g_1 because $g_1 L_{ov} \approx Z_c$ near the transition. Thus, a maximum in g_1 corresponds to a minimum in L_{ov}, and the divergence in g_1 at the transition corresponds to the vanishing of the overlap distance[9] as $L_{ov} \approx |\varphi - \varphi_c|^{1.0}$. Here we explored how the overlap distance, as measured by the height of the first peak of $g(r)$, evolves as a function of temperature near Point J.

In two-dimensional colloidal experiments, we probed the jamming transition at non-zero temperature by tuning the packing fraction. The experimental trajectory closely follows a horizontal line at fixed temperature in the $T - (1/\phi)$ plane above Point J in the jamming phase diagram (Fig. 1, dashed line). In parallel, we used three-dimensional simulations to explore the jamming transition in the same $T - (1/\phi)$ plane by two routes: (1) varying the packing fraction at fixed temperature (Fig. 1, dashed line) and (2) varying the temperature at fixed pressure (Fig. 1, dotted line).

The colloidal samples were aqueous suspensions of poly(N-isopropyl acrylamide) microgel colloidal particles (NIPA particles)[14,15], whose diameters increase substantially as temperature is reduced only slightly. Therefore, sample packing fraction could be tuned over a wide
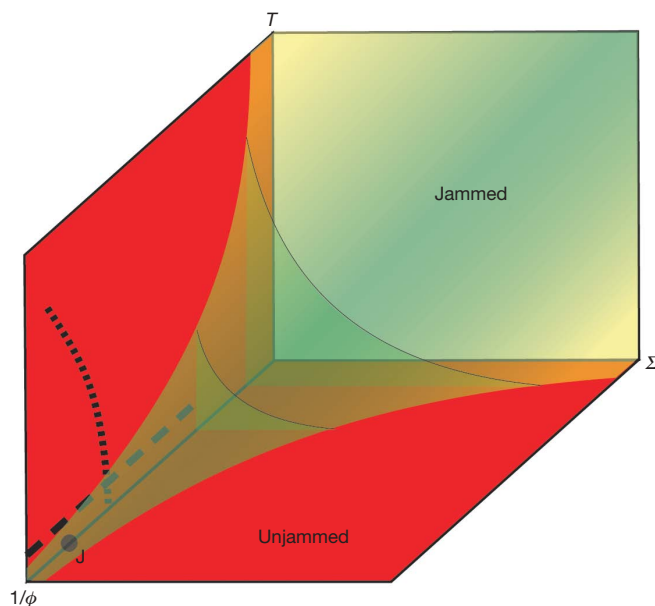

Figure 1 | Schematic jamming phase diagram. The surface of the green region in the three-dimensional space defined by temperature T, inverse packing fraction $1/\phi$ and applied stress Σ corresponds to the dynamical glass transition; within the green region the system is out of equilibrium. The point marked J represents a phase transition that occurs as ϕ is increased while $T = 0$ and $\Sigma = 0$. In the experiments, we varied the packing fraction at nearly fixed temperature, along the horizontal dashed line. In the simulations, we vary both packing fraction at fixed temperature along the horizontal dashed line, and temperature at fixed pressure along the dotted curve.

[1]Department of Physics and Astronomy, University of Pennsylvania, Philadelphia, Pennsylvania 19104, USA. [2]James Franck Institute, University of Chicago, Chicago, Illinois 60637, USA. [3]Department of Physics, West Chester University, West Chester, Pennsylvania 19383, USA. [4]Department of Physics, Saint Joseph's University, Philadelphia, Pennsylvania 19131, USA.
*These authors contributed equally to this work.

230

range with only minimal changes of temperature. This class of suspension has been successfully used to model a variety of phase transitions[16–21]. In our experiments, approximately equal numbers of monodisperse small and large NIPA particles with room-temperature (25 °C) diameters of $\sigma_S = 1.17\ \mu m$ and $\sigma_L = 1.63\ \mu m$, respectively, were sandwiched between two glass cover slips to form a two-dimensional colloidal suspension. The particle interaction potentials were measured to be short-range repulsive with a soft tail (Supplementary Fig. S2). The use of binary mixtures reduces the possibility of crystallization[22,23] and the softness of the potential, in contrast to that of hard spheres, permits access to packing fractions above the jamming transition.

In most colloidal experiments the thermodynamic control variable is packing fraction. Temperature control elements on the microscope objective in our experiments permitted the packing fraction ϕ to be varied *in situ* from ~0.76 to ~0.93, that is, across the packing fraction of the $T = 0$ jamming transition at $\phi \approx 0.84$ for temperatures ranging from 24.0 °C to 30.0 °C. At each ϕ the sample was permitted to equilibrate for 1,200 s before measurements were taken. We then used standard video microscopy[24] and particle-tracking techniques[25] to obtain the particle positions and the particle displacements. By identifying particle size and position we computed the three distinct pair-correlation functions: g_{LL} associated with large particles only, g_{SS} associated with small particles only, and g_{LS} probing the correlation between large and small particles. Here we focus only on g_{LL}. Qualitatively similar results were obtained for the other two correlation functions (Supplementary Fig. S3).

Figure 2 shows g_{LL} as a function of packing fraction ϕ. A prominent first peak at a distance of approximately one large particle diameter was found at all ϕ. In the inset to Fig. 2 we plotted g_1, the height of the first peak of $g_{LL}(r)$, versus ϕ. We note that g_1 has a pronounced maximum at $\phi = 0.85$. We identify this maximum as a vestige of the divergence in $g(r)$ seen at Point J, the $T = 0$ jamming transition.

In parallel, we used molecular dynamics simulations to explore the maximum in g_1 as a function of T and ϕ. We performed simulations using 1,000 particles of mass m in a three-dimensional cubic box with periodic boundary conditions. The particles are taken from a 50:50 distribution of the two diameters σ_L and σ_S, with ratio $\sigma_L/\sigma_S = 1.4$. Particles i and j interact via a repulsive spring-like potential, $U(r_{ij}) = \varepsilon(1 - r_{ij}/d_{ij})^\alpha/\alpha$, if their separation r_{ij} is smaller than the sum of their radii (that is, if they overlap), and do not interact otherwise. We used two types of repulsive potentials: harmonic ($\alpha = 2$) and Hertzian ($\alpha = 5/2$). We express distance in units of σ_S, time in units of $\sqrt{m\sigma_S^2/\varepsilon}$, sample temperature T in units of ε and pressure in units of ε/σ_S^3. We note that the Hertzian form provides a reasonable fit to the experimentally measured pair potential for NIPA particles at low concentration, with $\varepsilon/T \cong 270$ for the large particles (Supplementary Fig. S2). Figure 3a shows the data from simulations for harmonic
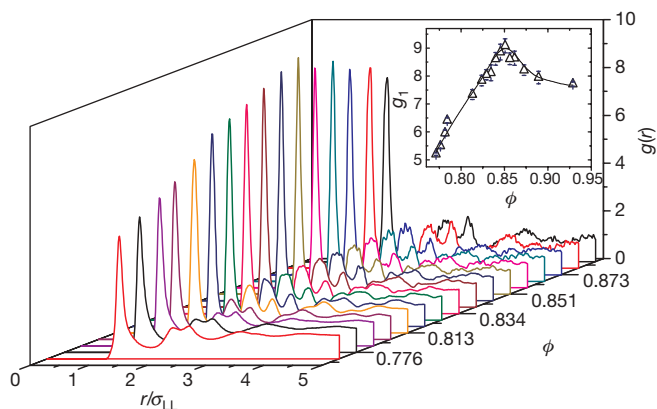
potentials at four temperatures that are analogous to our ϕ-dependent colloid experiments: g_1 is plotted versus $\Delta\phi \equiv \phi - \phi_c$, where ϕ_c is the onset of jamming at $T = 0$. The curve for each T exhibits a clear maximum, where $g_1 = g_1^{max}$, at $\Delta\phi_v(T)$ (subscript 'v' indicates vestige; inset to Fig. 3a). Thus, the constant-temperature three-dimensional simulation data are consistent with the colloidal experiments in two dimensions in that they both exhibit structural maxima as a function of packing fraction.

In both simulation and experiment, the value of g_1^{max} is finite and does not diverge as it does at Point J (refs 2, 9). In experiments, many factors can conspire to reduce g_1^{max}. In simulations, however, g_1^{max} is finite only because the temperature is not zero. Indeed, Fig. 3a shows that g_1^{max} decreases with increasing T as $g_1^{max} \propto (\Delta\varphi_v(T))^{-1}$, while its inset shows that $\Delta\phi_v(T)$ approaches zero as T tends to zero. This behaviour demonstrates that the maximum in g_1 at non-zero T evolves directly from the divergence in g_1^{max} at Point J.

The existence of a maximum in g_1 at finite temperature is easily understood. In the dilute limit, the height of the first peak increases with ϕ as more particles join the first-neighbour shell. At high ϕ, the first peak broadens with ϕ as the particles have greater overlap, leading to a drop in the peak height. We can predict the ϕ dependence of g_1^{max} as follows. At finite temperature, there are two contributions to the overlap between particles: (1) the static overlap L_O due to compression, which would exist even at $T = 0$, and (2) the additional overlap L_T
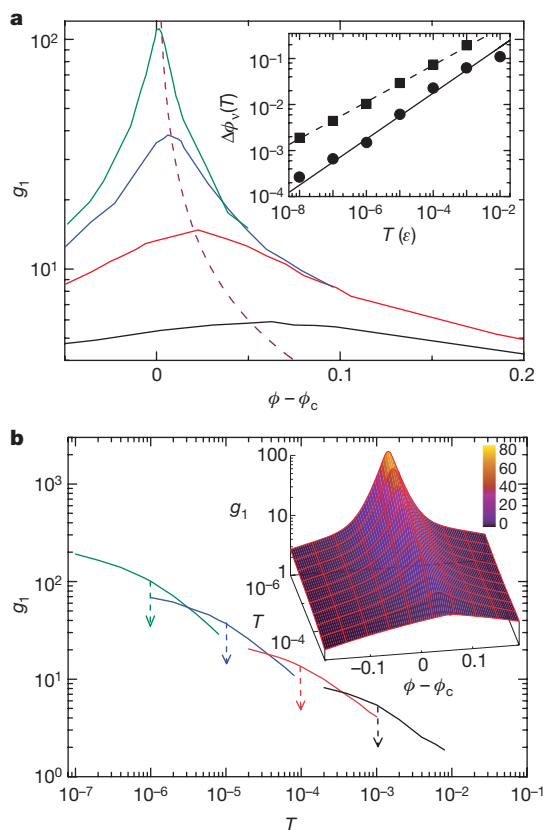
Figure 3 | Peak value of $g(r)$, g_1, measured from simulations. a, g_1 versus the packing fraction $\phi - \phi_c$, measured at temperatures $T = 10^{-3}\varepsilon$ (black), $10^{-4}\varepsilon$ (red), $10^{-5}\varepsilon$ (blue), and $10^{-6}\varepsilon$ (green), for harmonic interactions. The dashed line represents $g_1^{max} \propto \Delta\varphi^{-1}$, as expected theoretically. The inset shows $\Delta\phi_v(T)$, the location of the structural maximum for harmonic repulsions (circles) and Hertzian repulsions (squares). The solid and dashed lines are fits to the expected power-law scaling: $\Delta\phi_v \propto T^{1/\alpha}$ for $\alpha = 2$ and 5/2, respectively. **b**, g_1 versus T measured at constant pressures $P = 0.023\varepsilon/\sigma_S^3$ (black), $0.067\varepsilon/\sigma_S^3$ (red), $0.0017\varepsilon/\sigma_S^3$ (blue), and $0.00067\varepsilon/\sigma_S^3$ (green) with the arrows pointing to the temperatures at which g_1 reaches the maximum measured by varying the packing fraction at constant T as shown in **a**. The inset shows a three-dimensional plot of g_1 (colour scale) versus T and $\phi - \phi_c$.

Figure 2 | Pair-correlation function $g(r)$ for the large particles at all experimental packing fractions. The inset shows g_1, the height of the first peak of $g(r)$, as a function of packing fraction ϕ. The error bars in g_1 are the standard deviations of three independent calculations.

due to collisions arising from the (thermal) kinetic energy. The maximum in g_1 occurs when the spread in distances between neighbours is a minimum, which is typically when the total overlap, $L_{ov} = L_O + L_T$, is smallest. For sufficiently small T, the average potential energy per contact can be expanded as: $U(L_O + L_T) \cong U(L_O) + L_T \frac{dU}{dL}\Big|_{L=L_O}$. The system exhibits harmonic fluctuations around the energy minimum $U(L_O)$, so we have by equipartition that $U(L_O + L_T) - U(L_O) \propto T$. Note[2] that for a repulsive potential of the form $U(L) = \varepsilon L^{\alpha}$, we have $\frac{dU}{dL}\Big|_{L=L_O} \propto \Delta\phi^{\alpha-1}$ and $L_O \propto \Delta\varphi$ for sufficiently small $\Delta\phi$. Minimizing L_{ov} with respect to $\Delta\phi$ at fixed T therefore yields $\Delta\phi_v \propto T^{1/\alpha}$. The inset to Fig. 3a shows that this scaling is indeed observed in the simulations, confirming the view that the maximum in g_1 is a thermal structural vestige of the $T = 0$ jamming transition.

Although direct measurements of the pair-correlation function in three-dimensional colloidal systems have been made on colloidal glasses[26,27], to our knowledge the structural feature presented above has not been observed. A maximum in g_1 was observed in an athermal gas-fluidized granular system with increasing density at non-zero kinetic energy[28], with a second rise at the approach to random close-packing at zero kinetic energy. It is possible that the kinetic-energy/density trajectory of that experiment intersects the curve marking the evolution of the structural vestige with kinetic energy (or temperature) twice, once at the first local maximum and once at a second local maximum at Point J.

A maximum in g_1 was also not observed in scattering experiments on glass-forming liquids[29]. Such experiments extract positional information via measurements of the Fourier transform of the pair correlation function, the structure factor. One can readily show that a sharpening, or even a divergence of the first peak in $g(r)$, transforms into a signature in the structure factor that is spread over a wide range of wavevectors and is too subtle to be resolved with realistic experimental signal-to-noise conditions[2].

However, many simulations have searched for structural signatures of the glass transition in $g(r)$ (refs 22, 30). How could these simulations not have seen a maximum in the height of the first peak of $g(r)$? To answer this question, we conducted simulations along the more traditional phase-space trajectory, applicable to supercooled liquids and glasses, wherein temperature is varied as pressure (or packing fraction) is kept constant. Figure 3b shows that g_1 increases monotonically and does not exhibit a maximum when T is lowered at fixed pressure. Therefore, we do not see the structural vestige of Point J in a typical trajectory used to study the glass transition; we see a feature only when packing fraction or pressure is varied at fixed temperature. The behaviour of g_1 as a function of both T and ϕ is shown in the inset to Fig. 3b. Our observations are thus consistent with previous simulations, none of which explored trajectories at fixed temperature.

The systems studied here also exhibit classic dynamical glass transitions in which the structural relaxation time reaches the maximum timescale of the experiment or simulation. The dynamical glass transition lies at the boundary between the jammed and unjammed regions in the $T - (1/\phi)$ plane shown in the jamming phase diagram (Fig. 1). It is important to understand where the structural vestige of Point J, identified here from the structural maximum, lies in relation to the glass-transition line. To locate the dynamical glass transition in both the experiment and simulation, we measured the relaxation time τ_{α}, determined from the coherent intermediate scattering function (defined in the Supplementary Information). Experimentally, we found that τ_{α} increases rapidly with ϕ and eventually surpasses the experimental time window at $\phi_g \approx 0.85$, thus defining the packing fraction of the dynamical glass transition (Fig. 4a). This packing fraction coincides with the location of the maximum of g_1. Thus, in the colloidal experiment the thermal vestige of Point J occurs near the same packing fraction $\phi_v \cong 0.85$ as the dynamical glass transition so that $\phi_v \cong \phi_g$. However, this is not the case for the simulations, which
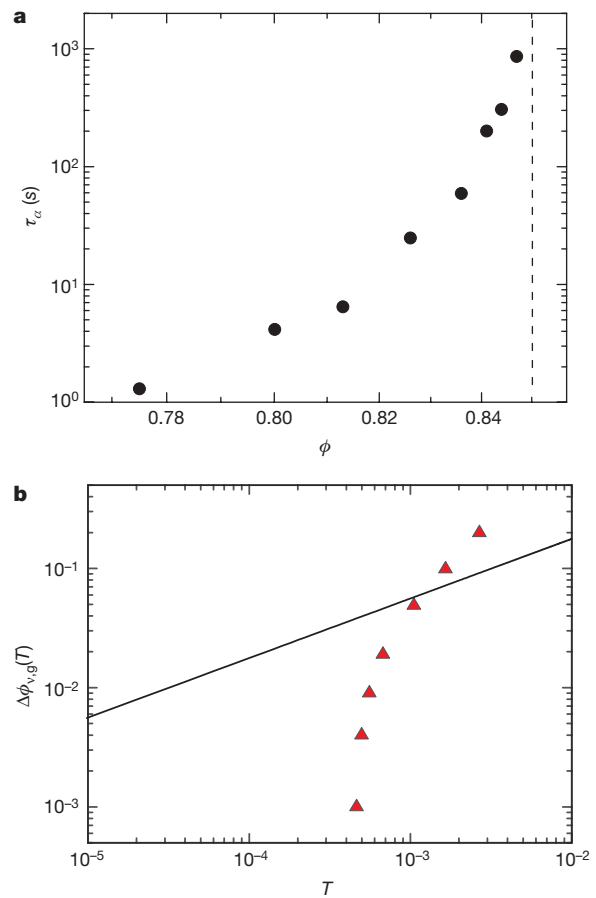
Figure 4 | Dynamics approaching the structural maximum. a, Experimental results for the α relaxation time τ_{α} for several packing fractions ϕ. The vertical dashed red line denotes the location of the structural maximum, determined from Fig. 2. **b,** Simulation results for $\Delta\phi_g(T)$ (red solid triangles), defined by where the relaxation time is equal to 10^4 in units of $\sqrt{m\sigma_S^2/\varepsilon}$, and $\Delta\phi_v(T)$ (black solid line, reproduced from the inset to Fig. 3a, corresponding to the power-law fit), the location of the structural maximum. Both $\Delta\phi_g(T)$ and $\Delta\phi_v(T)$ are calculated for harmonic repulsions ($\alpha = 2$).

can measure both ϕ_v and ϕ_g as a function of temperature. Thus, the experimental observation that $\phi_v \cong \phi_g$ appears to be a coincidence.

To demonstrate this in our simulations, we find the packing fraction of the dynamical glass transition, $\Delta\phi_g \equiv \phi_g - \phi_c$ for each temperature T at which τ_{α} exceeds the measurable window. In Fig. 4b we compare $\Delta\phi_g(T)$ to $\Delta\phi_v(T) \equiv \phi_v(T) - \phi_c$, the location of the structural vestige of jamming transition. At low temperatures, $\Delta\phi_g(T) < \Delta\phi_v(T)$, whereas at higher temperatures, $\Delta\phi_g(T) > \Delta\phi_v(T)$. In cases where the jamming transition lies in the out-of-equilibrium regime of Fig. 1, we find that g_1 and $\Delta\phi_v(T)$ are very robust to sample history. Rapidly quenched samples do age slightly, but settle down to a value of g_1 consistent with the results for slow quenches. Thus the vestige is neither a structural signature of the glass transition nor an artefact of falling out of equilibrium.

To conclude, we studied jamming in thermal systems in the vicinity of Point J. We found a maximum in the height of the first peak of the pair-correlation function that shifts to higher packing fractions as the temperature is increased from zero as $\Delta\phi_v \propto T^{1/\alpha}$, where α characterizes the inter-particle potential. This maximum is a vestige of one of the most important length scales that define the zero-temperature jamming transition at Point J (that is, the overlap length L_{ov} between neighbours). At Point J, this length scale vanishes because the system is isostatic and on the brink of mechanical failure. The present work shows that the evolution of the jamming transition with temperature is now accessible to experimental attack in colloidal systems. For

example, the evolution of two other diverging lengths at Point J, derived from the density of vibrational states and the elastic moduli[2], could be followed by experiment because the density of normal modes of vibration can, in principle, be measured from the Fourier transformation of the displacement of an individual particle in a colloidal sample. These length scales hold the possibility of connection to the glass transition, given that diverging timescales are often associated with diverging length scales. Our observations therefore demonstrate that length scales associated with the $T = 0$ jamming transition persist at non-zero temperatures, and also provide a route for using colloids to explore the relationship between Point J and the glass transition.

1. O'Hern, C. S., Langer, S. A., Liu, A. J. & Nagel, S. R. Random packings of frictionless particles. *Phys. Rev. Lett.* **88**, 075507 (2002).
2. O'Hern, C. S., Silbert, L. E., Liu, A. J. & Nagel, S. R. Jamming at zero temperature and zero applied stress: The epitome of disorder. *Phys. Rev. E* **68**, 011306 (2003).
3. Drocco, J. A., Hastings, M. B., Reichhardt, C. J. O. & Reichhardt, C. Multiscaling at point J: Jamming is a critical phenomenon. *Phys. Rev. Lett.* **95**, 088001 (2005).
4. Ellenbroek, W. G., Somfai, E., van Hecke, M. & van Saarloos, W. Critical scaling in linear response of frictionless granular packings near jamming. *Phys. Rev. Lett.* **97**, 258001 (2006).
5. Olsson, P. & Teitel, S. Critical scaling of shear viscosity at the jamming transition. *Phys. Rev. Lett.* **99**, 178001 (2007).
6. Silbert, L. E., Liu, A. J. & Nagel, S. R. Vibrations and diverging length scales near the unjamming transition. *Phys. Rev. Lett.* **95**, 098301 (2005).
7. Wyart, M., Silbert, L. E., Nagel, S. R. & Witten, T. A. Effects of compression on the vibrational modes of marginally jammed solids. *Phys. Rev. E* **72**, 051306 (2005).
8. Xu, N., Vitelli, V., Wyart, M., Liu, A. J. & Nagel, S. R. Energy transport in jammed sphere packings. *Phys. Rev. Lett.* **102**, 038001 (2009).
9. Silbert, L. E., Liu, A. J. & Nagel, S. R. Structural signatures of the unjamming transition at zero temperature. *Phys. Rev. E* **73**, 041304 (2006).
10. Donev, A., Torquato, S. & Stillinger, F. H. Pair correlation function characteristics of nearly jammed disordered and ordered hard-sphere packings. *Phys. Rev. E* **71**, 011105 (2005).
11. Liu, A. J. & Nagel, S. R. Nonlinear dynamics—Jamming is not just cool any more. *Nature* **396**, 21–22 (1998).
12. Trappe, V., Prasad, V., Cipelletti, L., Segre, P. N. & Weitz, D. A. Jamming phase diagram for attractive particles. *Nature* **411**, 772–775 (2001).
13. Durian, D. J. Foam mechanics at the bubble scale. *Phys. Rev. Lett.* **75**, 4780–4783 (1995).
14. Pelton, R. Temperature-sensitive aqueous microgels. *Adv. Colloid Interf. Sci.* **85**, 1–33 (2000).
15. Saunders, B. R. & Vincent, B. Microgel particles as model colloids: theory, properties and applications. *Adv. Colloid Interf. Sci.* **80**, 1–25 (1999).
16. Senff, H. & Richtering, W. Temperature sensitive microgel suspensions: Colloidal phase behavior and rheology of soft spheres. *J. Chem. Phys.* **111**, 1705–1711 (1999).
17. Wu, J. Z., Zhou, B. & Hu, Z. B. Phase behavior of thermally responsive microgel colloids. *Phys. Rev. Lett.* **90**, 048304 (2003).
18. Lyon, L. A. *et al.* Microgel colloidal crystals. *J. Phys. Chem. B* **108**, 19099–19108 (2004).
19. Alsayed, A. M., Islam, M. F., Zhang, J., Collings, P. J. & Yodh, A. G. Premelting at defects within bulk colloidal crystals. *Science* **309**, 1207–1210 (2005).
20. Han, Y., Ha, N. Y., Alsayed, A. M. & Yodh, A. G. Melting of two-dimensional tunable-diameter colloidal crystals. *Phys. Rev. E* **77**, 041406 (2008).
21. Han, Y. L. *et al.* Geometric frustration in buckled colloidal monolayers. *Nature* **456**, 898–903 (2008).
22. Kob, W. & Andersen, H. C. Testing mode-coupling theory for a supercooled binary Lennard-Jones mixture—The Van Hove correlation-function. *Phys. Rev. E* **51**, 4626–4641 (1995).
23. Perera, D. N. & Harrowell, P. Relaxation dynamics and their spatial distribution in a two-dimensional glass-forming mixture. *J. Chem. Phys.* **111**, 5441–5454 (1999).
24. Murray, C. A. & Grier, D. G. Video microscopy of monodisperse colloidal systems. *Annu. Rev. Phys. Chem.* **47**, 421–462 (1996).
25. Crocker, J. C. & Grier, D. G. Methods of digital video microscopy for colloidal studies. *J. Colloid Interf. Sci.* **179**, 298–310 (1996).
26. Kegel, W. K. & van Blaaderen, A. Direct observation of dynamical heterogeneities in colloidal hard-sphere suspensions. *Science* **287**, 290–293 (2000).
27. Weeks, E. R., Crocker, J. C., Levitt, A. C., Schofield, A. & Weitz, D. A. Three-dimensional direct imaging of structural relaxation near the colloidal glass transition. *Science* **287**, 627–631 (2000).
28. Abate, A. R. & Durian, D. J. Approach to jamming in an air-fluidized granular bed. *Phys. Rev. E* **74**, 031308 (2006).
29. Busse, L. E. & Nagel, S. R. Temperature-dependence of the structure factor of As_2Se_3 glass up to the glass-transition. *Phys. Rev. Lett.* **47**, 1848–1851 (1981).
30. Lacevic, N., Starr, F. W., Schroder, T. B., Novikov, V. N. & Glotzer, S. C. Growing correlation length on cooling below the onset of caging in a simulated glass-forming liquid. *Phys. Rev. E* **66**, 030101 (2002).